PRZEGLĄD ELEKTROTECHNICZNY

OPEN ACCESS

Muhamad Faizal YAAKUB[1], Mohd Amran MOHD RADZI[2], Norhafiz AZIS[3], Suhaidi SHAFIE[4], Maaspaliza AZRI[5], Faridah Hanim MOHD NOH[6]

ORCID: [1]0000-0002-8246-7397, [2]0000-0003-3785-1573, [3]0000-0002-9669-569X, [4]0000-0002-8867-2754, [5]0000-0001-9863-3241, [6]0000-0001-5328-6098

DOI: 10.15199/48.2026.3.26

An Impedance-Matching Technique for Suppressing Spurious Switching in Flyback Converters with Parasitic Effects

Technika dopasowania impedancji do tłumienia niepożądanych przełączeń w przetwornicach flyback z efektem pasożytniczym

[1] Muhamad Faizal Yaakub, Faculty of Electrical Technology and Engineering, Universiti Teknikal Malaysia Melaka, Hang Tuah Jaya, 76100 Durian Tunggal, Melaka, Malaysia, e-mail: muhamadfaizal@utem.edu.my

[2] Prof. Dr. Mohd Amran bin Mohd Radzi, Faculty of Engineering, Universiti Putra Malaysia, 43400 Serdang, Selangor, Malaysia, e-mail: amranmr@upm.edu.my

[3] Assoc. Prof. Dr. Norhafiz Azis, Faculty of Engineering, Universiti Putra Malaysia, 43400 Serdang, Selangor, Malaysia, e-mail: norhafiz@upm.edu.my

[4] Prof. Dr. Suhaidi Shafie, Faculty of Engineering, Universiti Putra Malaysia, 43400 Serdang, Selangor, Malaysia, e-mail: suhaidi@upm.edu.my

[5] Dr. Maaspaliza Azri, Faculty of Electrical Technology and Engineering, Universiti Teknikal Malaysia Melaka, Hang Tuah Jaya, 76100 Durian Tunggal, Melaka, Malaysia, e-mail: maaspaliza@utem.edu.my

[6] Dr. Faridah Hanim Mohd Noh, Faculty of Engineering Technology, Universiti Tun Hussein Onn Malaysia, 86400 Parit Raja, Johor, Malaysia, e-mail: hanim@uthm.edu.my

Correspondence address: muhamadfaizal@utem.edu.my

Abstract: The inherent galvanic isolation offered by flyback-based converters has attracted considerable interest across various applications, particularly in photovoltaic inverter systems. Despite all the advantages, the presence of parasitic elements introduces a significant design challenge. Distorted primary current at high-frequency switching can unintentionally trigger spurious switching pulses at the converter's main switch which caused the converter operation changes unpredictably. A new impedance-match technique for the enhanced topology is suggested to address the issue by exploiting the frequency-dependent characteristics of inductance within the parallel circuit and the behavior of the flyback's input impedance. A comprehensive analysis of the critical component selection is provided and the effectiveness of the proposed approach is validated and presented through experimental work on a developed 100-Watt laboratory prototype.

Keywords: flyback converter, impedance-matching, parasitic element, primary current

Streszczenie: Wrodzona izolacja galwaniczna oferowana przez przetwornice oparte na flyback przyciągnęła znaczne zainteresowanie w różnych zastosowaniach, szczególnie w systemach inwerterów fotowoltaicznych. Pomimo wszystkich zalet, obecność elementów pasożytniczych wprowadza znaczące wyzwanie projektowe. Zniekształcony prąd pierwotny przy przełączaniu wysokiej częstotliwości może nieumyślnie wywołać fałszywe impulsy przełączające na głównym przełączniku przetwornicy, co powoduje nieprzewidywalne zmiany w działaniu przetwornicy. Zaproponowano nową technikę dopasowania impedancji dla ulepszonej topologii, aby rozwiązać ten problem poprzez wykorzystanie zależnych od częstotliwości charakterystyk indukcyjności w obwodzie równoległym i zachowania impedancji wejściowej flyback. Przedstawiono kompleksową analizę krytycznego wyboru komponentów, a skuteczność proponowanego podejścia została zweryfikowana i przedstawiona poprzez prace eksperymentalne na opracowanym 100-watowym prototypie laboratoryjnym.

Słowa kluczowe: przetwornica flyback, dopasowanie impedancji, element pasożytniczy, prąd pierwotny

Introduction

A flyback dc-dc converter is widely utilized in photovoltaic (PV) inverter application, particularly to boost DC voltage from a PV panel to a different voltage level. Its on-board transformer is crucial to provide essential galvanic isolation [1]–[3]. However, the transformer is normally designed for a specific rating with narrow tolerance of switching frequencies, limit-

ing its flexibility especially in variable switching frequency application[4], [5].

Peak-current control (PCC), implemented in conjunction with boundary conduction mode (BCM) has emerged as a widely adopted control strategy in flyback converters, which inherently features variable switching frequency in high power density application. However, this combination faces a notable challenge where the interaction of parasitic element within the circuit generates overshoot and oscillation at the primary/input signal, particularly the current. The distortion is pronounced at the edge of the PCC reference signal, where the switching frequency can rise to several hundred kilohertz, significantly increasing the risk of false switching events [6]–[9]. A thorough investigation was conducted in earlier work to assess the influence of parasitic elements on a flyback converter over a broad range of switching frequencies [10], [11]. Simulation and experimental studies indicate that the characteristics of the flyback transformer vary with changes in the switching frequency. As the self-resonance frequency (SRF) decreased with increasing frequency, the transformer's behaviour shifted from inductive to capacitive mode. Consequently, inducing a distortion in the primary current.

Numerous studies have proposed techniques to address the interferences challenge caused by the high switching frequency in these critical area, using approaches such as algorithm-based switching control methods [5][12]–[14]. Additional strategies to encounter parasitic effects include diode-clamp circuits combined with series resonant inductors [15] and parallel resonant capacitors [16]. However, the outcomes of these methods vary substantially based on their specific intended applications.

In this paper, an enhanced circuit arrangement for the flyback converter is presented and introduces a new technique specifically aimed at compensating for parasitic effects and significantly improves the converter's primary current behavior during high-frequency operation under PCC, especially in scenarios involving variable switching frequencies.

Methodology

Given that the primary current is directly influenced the switching mechanism in PCC, the proposed enhanced circuit arrangement is developed to attain the desired undistorted current signal. Fig. 1 illustrates the flyback converter schematic with the enhanced auxiliary circuit. It consists of an inductor connected in parallel with the transformer primary winding. Additional components, connected in series such as the diode, used to ensure unidirectional current flow, while the switching device will engage the auxiliary as needed. The auxiliary inductor is fundamentally derived from the behavior of an inductive circuit, where the inductor's reactance is directly proportional to the operational frequency. Keeping the reactance constant, the inductance exhibits its inverse proportional relationship with the frequency, as shown in equation (1) and (2).

$$X_L = 2\pi f L \tag{1}$$

$$L = \frac{X_L}{2\pi f} \tag{2}$$

Early investigation reveals that the impedance of the transformer in the converter is shifted at high-frequency switching operation [10]. This led to behavioral changes due to activation of the parasitic elements. Hypothetically, by maintaining the impedance at transformer operational frequency, the behavior will remain unchanged and the interference can be eliminated or extremely minimized during high-frequency switching operation. Therefore, according to equation (2), it can be achieved by adjusting the inductance value at the primary side of the converter. Taking into account the impedance at operation rated switching frequency as a reference, Z_{in_ref}, equation (3) is modified to acquire the auxiliary inductance value, L_{ax} as shown in equation (4).

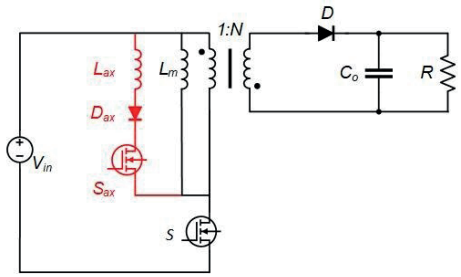

Fig. 1. Flyback DC-DC converter with proposed enhanced auxiliary circuit

$$Z_{in_ref} = \sqrt{\frac{L_{m_opr}}{C_{eq_opr}}} \tag{3}$$

where L_{m_opr} and C_{eq_opr} are the transformer's magnetizing inductance and the equivalent capacitance at rated operational frequency, respectively.

$$L_{ax} = \frac{Z_{in_ref}^2 L_{p_HF} C_{eq_HF}}{L_{p_HF} - \left(Z_{in_ref}^2 C_{eq_HF}\right)} \tag{4}$$

where:
L_{ax} – is the auxiliary inductance,
L_{p_HF} and C_{eq_HF} – are the transformer's primary inductance and equivalent capacitance at high-frequency operation, respectively.

Operational analysis

When the switching frequency reaches the threshold, the auxiliary circuit's low-side switch is activated, allowing L_{ax} to couple with the transformer. At this point, L_m and L_{ax} combine to form the equivalent inductance, L_{Mx}. The operational waveforms and corresponding equivalent circuits for each interval are presented in Fig. 2 and Fig. 3, respectively.

Interval 1 (t_0- t_1): The main switch, S, is ON before switching at time t_0. When S turns OFF at $t = t_0$, L_{Mx} begins discharging C_q. Resonance between C_q and L_{Mx} delays energy transfer to the secondary winding until C_q reaches $-V_o/N$ at time $t = t_1$. The current through the magnetizing-auxiliary inductance peaks at t_{01}. The magnetizing-auxiliary current during this period can be mathematically expressed as:

$$(5)\quad i_{L_{Mx}}(t) = \frac{V_{in}}{Z_i}\sin(\omega_r t) + I_{LMx_t0}\cos(\omega_r t)$$

Where I_{Lmx_t0} is current flowing through L_{Mx} at switch off. $Z_i=(L_{Mx}/C_q)^{1/2}$ and $\omega_r= 1/(L_{mx} \cdot C_{eq})^{1/2}$.

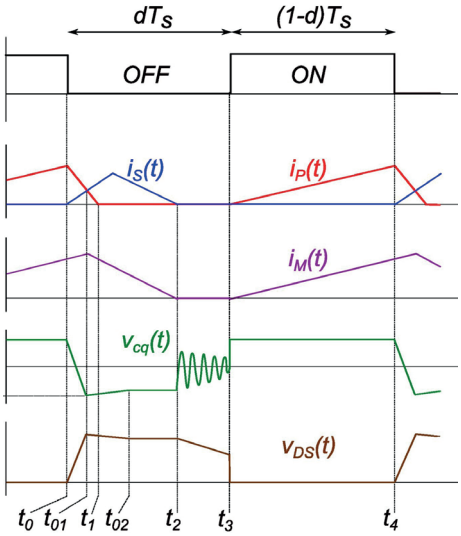

Fig. 2. Proposed enhanced theoretical waveform

Interval 2 (t_1 – t_2): When the capacitor voltage, V_{cq}, drops to $-V_o/N$ at time t_1, the secondary-side diode, D, starts conducting. This allows current from L_{Mx} to flow to the output side. During this interval, V_{cq} rises until the main switch voltage reaches $V_{in} + (N_1/N_2)V_o$ at t_{02}. Afterward, V_{cq} holds steady while the L_{Mx} current, I_{LMx}, gradually decreases and reaches zero at t_2. The current decline can be mathematically expressed by

$$(6)\quad i_{L_{Mx}}(t) = -\frac{V_o}{NL_{Mx}}(t - t_1) + I_{LMx_{t1}}$$

Where V_o is the converter's output voltage, and I_{LMt1} is the current through L_{Mx} at time t_1.

Interval 3 (t_2 – t_3): A resonance circuit forms through C_q, C_{S_oss}, C_{D_Oss}, L_{Mx}, and L_{lk} after L_{Mx} fully transfers its energy to the secondary side. At this point, the initial voltage across C_q reverses, changing its polarity. Meanwhile, the secondary-side diode stops conducting when I_{LMx} reaches zero. However, the switch voltage does not immediately fall to zero. The interaction between L_{Mx} and C_q creates a quasi-resonant state, helping V_{ds} reach zero at time t_3. As a result, the anti-parallel diode of the primary switch, S, begins conducting, enabling zero-voltage switching (ZVS). The magnetizing current and voltage across the equivalent capacitance are given by

$$(7)\quad i_{L_M}(t) = -\frac{V_o}{NZ_i}\sin(\omega_r t)$$

$$(8)\quad v_{C_{eq}}(t) = -\frac{V_o}{N}\cos(\omega_r t)$$

This interval ends when the voltage across the equivalent capacitance, V_{ceq}, reaches V_{in} at t_3.

Interval 4 (t_3 – t_4): During this interval, switch S is turned ON. The energy is stored in L_{Mx} through the path V_{in} – L_{Mx} – S. As a result, the primary-side current increases linearly. The magnetizing-auxiliary current is given by:

$$(9)\quad i_{L_{Mx}}(t) = \frac{V_i}{L_{Mx}}(t - t_3) + I_{LMx_{t3}}$$

I_{Lmxt3} is the instantaneous i_{LMx} at the start of this interval. The current at t_4 eventually equals the current at t_0. Thus, based on equation (7), equation (9) can be derived as:

$$(10)\quad i_{L_{Mx}}(0) = \frac{V_i}{L_{Mx}}(t_4) + I_{LMx_{t3}}$$

$$= \frac{V_i}{Z_i}(\omega_r t_4) - \frac{V_o V_i}{NZ_i V_i}\sin(\omega_r t_3)$$

This interval ends when the primary switch S is turned OFF.

Experimental setup and verification

To validate the previously established theoretical hypothesis, A 100 W laboratory prototype was built, based on the overall structure as depicted in Fig. 4, with specification listed in Table 1. The switching pulse for the main switch and the enable signal for the auxiliary path were programmed using the CMPSS and ePWM modules of a TMS320F28379D DSP board from Texas Instruments. Experiments were conducted at fixed switching frequency of 200 kHz, as well as variable switching frequency through PCC.

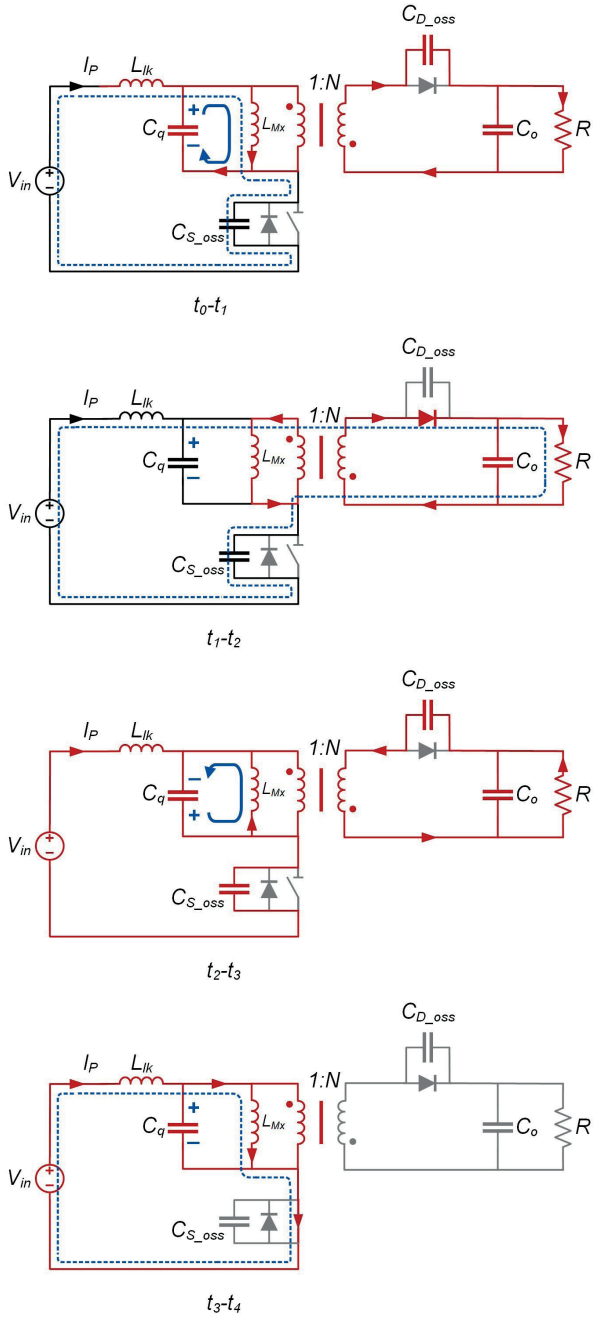

Fig. 3. Equivalent operational circuit at each time interval

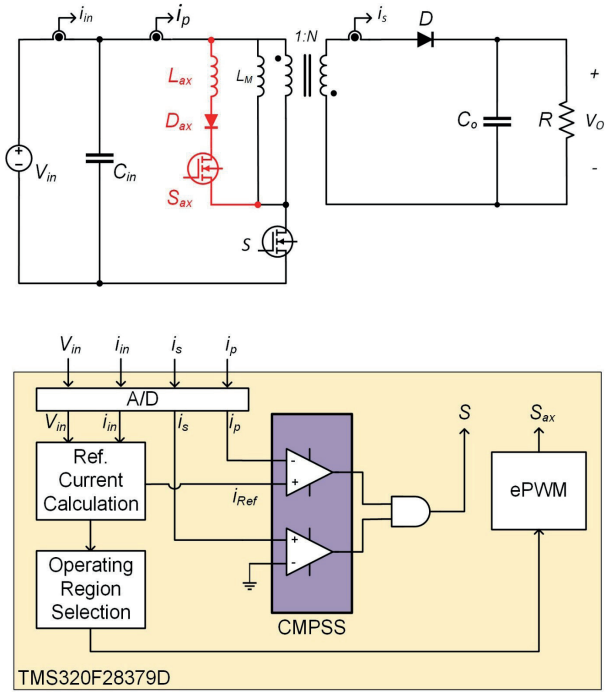

Fig. 4. Overall structure of experimental setup

Fixed switching frequency, 200 kHz for hardware verification were chosen based on the influence of parasitic components and the preliminary analysis of the transformer's self-resonant frequency (SRF)[10], [11]. Fig. 5 shows the measured primary current yielded from the stimulus switching pulse with implemented proposed approach at 200 kHz. For comparison, the current profiles prior to the proposed method are shown in Fig. 6, where the peak current value is around 3 A. As can be seen, the proposed approach shifts the operation of the converter from CCM to DCM and successfully eliminated the oscillation at primary current with new peak at 15 A and 8 A. The enhancement is attributed to the reduction of spurious switching events resulting from parasitic capacitances and leakage inductances, which commonly produce high-frequency oscillations and contribute to additional switching losses. The proposed network minimizes reflected parasitic effects by matching the impedance between the primary and secondary circuits, which results in a reduction of both conduction and switching power losses. This improvement somehow aligned with [15], who reported a similar improvement by proposing a clamp diode solution. However, unlike their study, which focus on the average current value at fixed switching frequency, the improvement made by the proposed approach extends to provide a simpler control approach for close loop operation and suit for light-load peak current regulation under PCC and variable switching frequency.

When a rectified sinusoidal-like waveform is used as the PCC current reference in a closed-loop system, the switching frequency tends to increase at the beginning and end of each reference signal period. As shown in Fig. 7, distortion in the primary current of the flyback converter can unintentionally trigger spurious switching pulses at the converter's main switch. These irregular pulses result in inconsistent duty cycles, causing the converter operation to shift unpredictably between DCM and CCM. In contrast, Fig. 8 illustrates the improvement made by the proposed auxiliary inductor, where periodic switching pulses are consistently triggered. A uniform switching pattern with a 50% duty cycle is observed at the edge of the reference current waveform, corresponding to a measured switching frequency of 200 kHz.

Table 1. Key parameters of the enhanced flyback converter

Parameter/device	Symbol	Value
Flyback Transformer	T_x	Coil Craft NA5814-AL
Main Switch	S	UF3C065080T3S 650V-80mΩ SiC FET
Power Coupling Capacitor	C_{in}	Electrolytic capacitors of 2200uF, 63 V
Power Diode	D	IDH06G65C6 650V SiC Schottky Diode
Output Capacitor	C_o	480uF, 400V
Resistive Load	R	500 Ω
Aux. Inductance	L_{ax}	4 μH ~ 18 μH
Aux. Switch	S_{ax}	FCP22N60N MOSFET
Aux. Diode	D_{ax}	RK34 Si Schottky
Nom. Input Voltage	V_{in}	20 V
Rated Output Power	P_{rated}	100 W
Fixed Switching Freq	F_{sw}	200 kHz

Table 2 tabulates the measured parameters under BCM PCC with and without L_{ax} activated. Activation of the auxiliary inductor L_{ax} results in a peak efficiency of 95.8% for the converter, in contrast to 92.7% when L_{ax} is deactivated, indicating a relative improvement of 3.1%. From a power balance perspective, the input power P_{in} decreases from 42.39 W to 39.79 W, while the output power P_{out} remains relatively constant at 39.3 W compared to 38.1 W. The reduction in power loss, $\Delta P_{loss}=P_{in}-P_{out}$, is primarily attributed to the mitigation of parasitic resonances and circulating currents. The output current I_o is well-regulated, decreasing from 305 mA to 300 mA, while the output voltage remains stable within the range of 127–129 V, indicating effective voltage regulation under the proposed approach.

Table 2. Measured power and efficiency of the proposed method under PCC

L_{ax} status	V_{in} (V)	I_{in} (A)	V_o (V)	I_o (mA)	P_{in}	P_{out}	η(%)
ON	19.7	2.02	127	300	39.79	38.1	95.8
OFF	19.9	2.13	129	305	42.39	39.3	92.7

Table 3. Measured power and efficiency of the proposed method under fixed frequency, F_{sw} = 200 kHz

L_{ax} status	V_{in} (V)	I_{in} (A)	V_o (V)	I_o (mA)	P_{in}	P_{out}	η(%)
ON	19.2	1.62	88	327	31.10	28.8	92.6
OFF	19.4	1.70	85	330	32.9	28.05	85.1

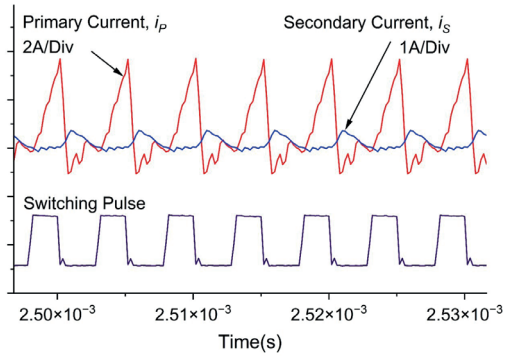

Fig. 5. Flyback converter primary current with proposed approach at 200 kHz

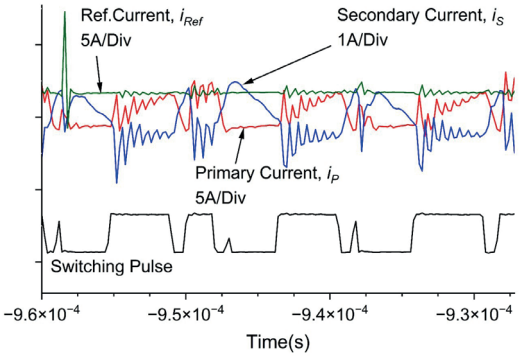

Fig. 7. Spurious switching pulse resulted from distorted primary current under PCC

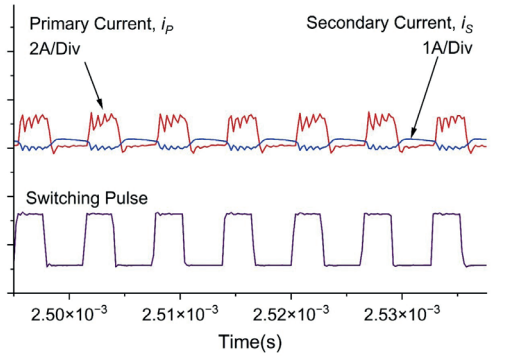

Fig. 6. Flyback primary converter primary current under parasitic influence at 200 kHz

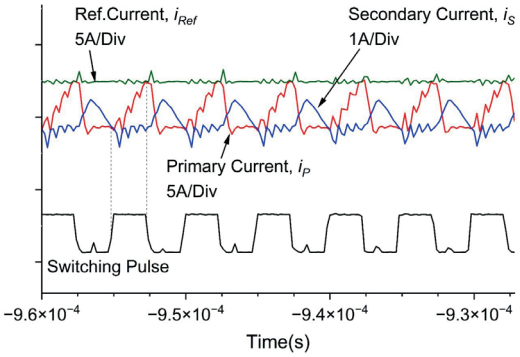

Fig. 8. Improved switching cycle under PCC by the proposed auxiliary inductor

Under fixed-frequency operation at F_{sw}=200 kHz, activating L_{ax} decreases the input current from 1.70 A to 1.62 A, resulting in a reduction of input power from 28.8 W to 28.05 W, as shown in Table 3. This corresponds with the fundamental equation $P_{in}=V_{in}\times I_{in}$, signifying decreased conduction and switching losses. The efficiency increases from 85.1% to 92.6%, demonstrating the efficacy of the impedance-matching network in sustaining stable switching transitions under constant frequency.

Although the average output current is little bit lower with the proposed approach, this is already expected since the converter consistently operate at DCM or BCM at most. Compared when without the auxiliary inductor, the converter also operates at CCM which produce anticipate higher output current.

Conclusion

This paper introduces a novel technique for input impedance matching in flyback converters, designed to reduce parasitic effects and suppress unwanted switching events. The proposed method incorporates an auxiliary resonant inductor in parallel with the primary winding of the transformer and its equivalent parasitic capacitance, utilizing the core principles of inductive circuit behavior. This configuration stabilizes the input impedance over a broad range of switching frequencies, ensuring that the input current is undistorted and devoid of resonance-induced distortions. The technique effectively reduces high-frequency oscillations and related switching losses by minimizing the effects of leakage inductance and parasitic capacitance. Experimental results confirm that the method enhances overall energy conversion efficiency by reducing conduction and switching losses while ensuring stable output voltage and current regulation, even in dynamic operating conditions.

Acknowledgements: *The authors would like to thank Universiti Teknikal Malaysia Melaka and Universiti Putra Malaysia for their financial and technical support.*

Received: 11.05.2025, **Accepted:** 18.12.2025, **Published:** 26.03.2026

REFERENCES

[1] M. Srinivasan, "Analysis and stabilization of CCM flyback converters supplying constant power loads," in 2021 IEEE Kansas Power and Energy Conference (KPEC), 2021, pp. 1–6. doi: 10.1109/kpec51835.2021.9446229.

[2] E. E. Henao-Bravo, C. A. Ramos-Paja, A. J. Saavedra-Montes, D. González-Montoya, and J. Sierra-Pérez, "Design method of dual active bridge converters for photovoltaic systems with high voltage gain," Energies, vol. 13, no. 7, pp. 1–31, 2020, doi: 10.3390/en13071711.

[3] A. Boyar and E. Kabalci, "Two-Stage Flyback Micro Inverter for Solar Power Conversion," Proc. - 2020 IEEE 2nd Glob. Power, Energy Commun. Conf. GPECOM 2020, pp. 6–11, 2020, doi: 10.1109/GPECOM49333.2020.9247905.

[4] I. Variable, S. Tal, and T. Garcia, "(12) United States Patent (10) Patent No.:," vol. 2, no. 12, 2011.

[5] M. Gao, M. Chen, C. Zhang, and Z. Qian, "Analysis and implementation of an improved flyback inverter for photovoltaic AC module applications," IEEE Trans. Power Electron., vol. 29, no. 7, pp. 3428–3444, 2014, doi: 10.1109/TPEL.2013.2279266.

[6] G. C. Christidis, A. C. Nanakos, and E. C. Tatakis, "Hybrid Discontinuous/Boundary Conduction Mode of Flyback Microinverter for AC-PV Modules," IEEE Trans. Power Electron., vol. 31, no. 6, pp. 4195–4205, 2016, doi: 10.1109/TPEL.2015.2470094.

[7] S. Kim, S. H. Lee, J. S. Lee, and M. Kim, "Dual-mode flyback inverters in gridconnected photovoltaic systems," IET Renew. Power Gener., vol. 10, no. 9, pp. 1402–1412, 2016, doi: 10.1049/iet-rpg.2015.0491.

[8] T. Lodh, N. Pragallapati, and V. Agarwal, "Novel Control Scheme for an Interleaved Flyback Converter Based Solar PV Microinverter to Achieve High Efficiency," IEEE Trans. Ind. Appl., vol. 54, no. 4, pp. 3473–3482, 2018, doi: 10.1109/TIA.2018.2818655.

[9] C. C. Chuang, C. C. Hua, C. Y. Huang, and L. K. Jhou, "Modeling a dual-mode controller design for a quasi-resonant flyback converter," Appl. Sci., vol. 9, no. 9, 2019, doi: 10.3390/app9091860.

[10] M. F. Yaakub, M. Amran, M. Radzi, F. Hanim, and M. Noh, "Simulation of DC-DC Converter Considering Parasitic Element in Flyback Transformer and its Effect on the Converter ' s Input Current," 2023 IEEE 11th Conf. Syst. Process Control, vol. 1, no. December, pp. 182–187, 2023, doi: 10.1109/ICSPC59664.2023.10420409.

[11] M. F. Yaakub, M. Amran, M. Radzi, F. Hanim, M. Noh, and N. Azis, "Influence of Parasitic Elements on Flyback Converter at High Switching Frequency Operation : A Comprehensive Analysis," vol. 4, no. 4, pp. 188–199, 2024.

[12] S. J. Yaqoob et al., "Flyback Photovoltaic Micro-Inverter with a Low Cost and Simple Digital-Analog Control Scheme," Energies, vol. 14, 2021.

[13] S. Arab Ansari, J. S. Moghani, and M. Mohammadi, "Analysis and implementation of a new zero current switching flyback inverter," Int. J. Circuit Theory Appl., vol. 47, no. 1, pp. 103–132, 2019, doi: 10.1002/cta.2577.

[14] Z. Zhang, M. Chen, W. Chen, and Z. Qian, "Design and Analysis of the synchronization control method for BCM/DCM current-mode flyback micro-inverter," Conf. Proc. - IEEE Appl. Power Electron. Conf. Expo. - APEC, pp. 68–75, 2013, doi: 10.1109/APEC.2013.6520187.

[15] J. M. Jiménez-Martínez, E. de Jódar, and J. Villarejo, "Parasitic Capacitance Effects on Active Clamp Flyback Output Characteristics: Application to IPOP Connection," Energies, vol. 15, no. 9, 2022, doi: 10.3390/en15093201.

[16] S. S. Hong, S. K. Ji, Y. J. Jung, and C. W. Roh, "Analysis and design of a high voltage flyback converter with resonant elements," J. Power Electron., vol. 10, no. 2, pp. 107–114, 2010, doi: 10.6113/JPE.2010.10.2.107.